Real-life Measurement of Tri-axial Walking Ground Reaction Forces using Optimal Network of Wearable Inertial Measurement Units

Erfan Shahabpoor, Aleksandar Pavic, James M. W. Brownjohn, Stephen A. Billings, Ling-zhong Guo, Mateusz Bocian

Abstract—Monitoring natural human gait in real-life environment is essential in many applications including quantification of disease progression, and monitoring the effects of treatment and alteration of performance biomarkers in professional sports. Nevertheless, reliable and practical techniques and technologies necessary for continuous real-life monitoring of gait is still not available. This paper explores in detail the correlations between the acceleration of different body segments and walking ground reaction forces $GRF(t)$ in three dimensions and proposes three sensory systems, with one, two and three inertial measurement units (IMUs), to estimate $GRF(t)$ in the vertical (V), medial-lateral (ML) and anterior-posterior (AP) directions. The NARMAX non-linear system identification method was utilized to identify the optimal location for IMUs on the body for each system. A simple linear model was then proposed to estimate $GRF(t)$ based on the correlation of segmental accelerations with each other. It was found that, for the three-IMU system, the proposed model estimated $GRF(t)$ with average peak-to-peak normalized root mean square error (NRMSE) of 7%, 16% and 18% in V, AP and ML directions, respectively. With a simple subject-specific training at the beginning, these errors were reduced to 7%, 13% and 13% in V, AP and ML directions, respectively. These results were found favorably comparable with the results of the benchmark NARMAX model, with subject-specific training, with 0% (V), 4% (AP) and 1% (ML) NRMSE difference.

***Index Terms*— ambulation, biomechanics, black-box approach, gait monitoring, outdoor measurement.**

Submitted for review on 16 August 2017.

The authors acknowledge the financial support provided by the UK Engineering and Physical Sciences Research Council (EPSRC) for the following research grants:

- Frontier Engineering Grant EP/K03877X/1 (Modelling complex and partially identified engineering problems: Application to the individualized multi-scale simulation of the musculoskeletal system);
- Platform Grant EP/G061130/2 (Dynamic performance of large civil engineering structures: an integrated approach to management, design and assessment); and
- Great Technologies Capital Call, Robotics and Autonomous Systems EP/J013714/1 (Human-Machine Co-operation in Robotics and Autonomous Systems).

E. Shahabpoor was with the INSIGNEO Institute for In-silico Medicine, Department of Civil & Structural Engineering, University of Sheffield, Sheffield, United Kingdom. He is now with the Department of Architecture and Civil Engineering, University of Bath, Claverton Down, Bath, United Kingdom (e-mail: e.shahabpoor@bath.ac.uk).

A. Pavic is with the College of Engineering, Mathematics and Physical Sciences, University of Exeter, Exeter, United Kingdom.

J.M.W. Brownjohn is with the College of Engineering, Mathematics and Physical Sciences, University of Exeter, Exeter, United Kingdom.

S.A. Billings was with the Department of Automatic Control and Systems Engineering, University of Sheffield, Sheffield, United Kingdom.

L. Guo is with the INSIGNEO Institute for In-silico Medicine, Department of Automatic Control and Systems Engineering, University of Sheffield, Sheffield, United Kingdom.

M. Bocian is with the Department of Engineering, University of Leicester, University Road, Leicester, United Kingdom.

I. Introduction

Walking ground reaction forces $GRF(t)$ and moments are critical inputs for musculoskeletal modelling and gait analysis. Quantification of the spatiotemporal gait fluctuations over time or due to environmental, behavioral or contextual factors in real-life environment are essential in many applications such as understanding the motor control of gait, quantifying pathologic and age-related alterations in the locomotor control system, and augmenting objective measurement of mobility and functional status [1].

Several techniques and technologies have been developed in the past three decades to measure or estimate tri-axial $GRF(t)$ signals using wearable sensors. Inertial Measurement Units (IMUs) have been particularly an attractive sensory option for continuous measurement in real-life environment due to their small form factor, low power consumption, low cost and capability to measure orientation. Recently, McDonald and Zivanovic [2], and Bocian, et al., [3] suggested that the vertical acceleration measured using an IMU at 7th cervical vertebra ($\ddot{x}_{v,C7}(t)$) can be used to estimate the total jumping and walking ground reaction forces ($GRF_v(t)$) in the vertical direction, respectively. Both studies assume that $\ddot{x}_{v,C7}(t)$ represents the movement of the total body mass m_{total} lumped at the center of mass (CoM) of the body and, therefore, $GRF_v(t)$ can directly be estimated using (1):

$$GRF_v(t) = m_{total}\big(\ddot{x}_{v,C7}(t) + g\big), \tag{1}$$

where, g is the gravitational acceleration.

Later in 2017, Gurchiek, et al., [4] showed that a single IMU at Sacrum can be used to estimate the tri-axial $GRF(t)$ signals during accelerative running. These pioneering works highlight the possibility of estimating $GRF(t)$ signals from limited number of IMU measurements.

This paper proposes a linear model to estimate $GRF(t)$ signals from an optimal network of IMU sensors. An experimental dataset from six subjects (Section II) is used to analyze the correlations between the acceleration of different body

segments and $GRF(t)$ (Section III) and contribution of each segment to $GRF(t)$ signals in three dimensions (Section III). Section IV of the paper uses the NARMAX non-linear system identification method to find the optimal location on the body for IMUs for systems, with one, two and three sensors. For the locations identified for the three-IMU system, Section V proposes two linear models to estimate tri-axial $GRF(t)$ based on the correlation of segmental accelerations with each other. Section VI explores the improvements in the accuracy of the estimated $GRF(t)$ signals if non-linear models were used instead of linear models presented in Section V. Performance of the proposed model is analyzed in real-life (outside laboratory) environment in Section VII and the conclusions are presented in Section VIII and few suggestions are made for future research.

II. Experimental Campaign

Six healthy male subjects S1-S6 (age: 21±1years, weight: 77±16kg and height: 1.82±0.08m) participated in a set of walking gait measurement in the biomechanics laboratory at the University of Sheffield. The subjects provided an informed consent in accordance with the ethical guidelines for research involving human participants at the University of Sheffield. The normal walking speed of each subject was initially found, by trial and error, equal to $v_{w,S1} = 1.25m/s$, $v_{w,S2} = 1.28m/s$, $v_{w,S3} = 1.28m/s$, $v_{w,S4} = 1.11m/s$, $v_{w,S5} = 1.19m/s$ and $v_{w,S6} = 1.06m/s$. Then subjects S1-S4 each participated in a set of six walking tests with 180s duration, where the treadmill speed was set to 60%, 70%, 80%, 90%, 100% and 110% of their normal walking speed, respectively. Subjects S5 and S6 each did a single walking test only with their comfortable walking speed.

In each test, the full-body 3D motion data were recorded using CODA motion capture system [5] at 100Hz sampling rate. The marker placement protocol was based on full-body Plug-in Gait [6] (Fig. 1). The tri-axial walking $GRF(t)$ signals pertinent to each foot were recorded at 1kHz sampling rate using a bespoke grounded instrumented treadmill with two separate belts and six axis forceplates for each foot.

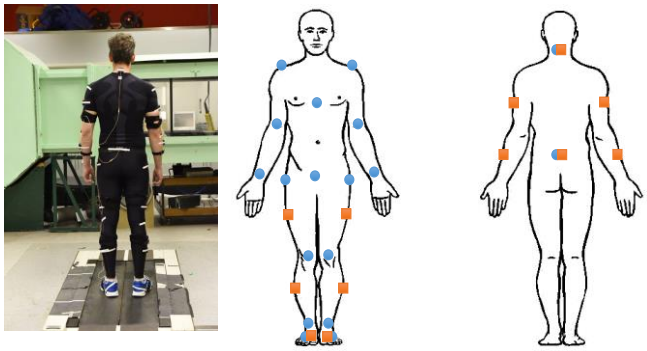

a) b)

Fig. 1. (a) Subject instrumentation layout and (b) location of the CODA markers (blue circles) and the Opal IMUs (orange squares)

A set of 12 Opal IMUs [7] were used to measure the tri-axial acceleration and orientation signals at 7th cervical vertebrae (C7), 5th lumbar vertebrae (L5), upper arms, fore arms, thighs, shanks and fourth metatarsals with 128Hz sampling rate (Fig. 1). Each IMU sensor was placed closest to the approximate location of CoM of the corresponding segment based on the anatomical locations suggested by Winter [1].

Three independent right-handed coordinate systems were considered: 1) the laboratory-fixed Cartesian coordinate system (LCS) which x_{LCS}, y_{LCS}, and z_{LCS} axes point towards magnetic East, North, and up (vertical) direction, respectively; 2) the body-fixed Cartesian coordinate system (BCS) where z_{BCS} axis points upwards in the vertical direction, y_{BCS} points towards walking direction (anterior), and x_{BCS} is perpendicular to y_{BCS} and z_{BCS}, towards right of the body to form the right-handed coordinate system. Both x_{BCS} and y_{BCS} axes are in the horizontal (transverse) plane; and 3) the IMU sensors local coordinate system (SCS) defined by x_{SCS}, y_{SCS}, and z_{SCS} axes.

The range of trunk motion, tilt, obliquity, and rotation around body-fixed coordinate axis x_{BCS}, y_{BCS}, and z_{BCS} during straight normal walking are approximately ±2°, ±1.5°, and ±3.5°, respectively [8]. However, in real-life walking, particularly during turning, the rotation around z_{BCS} can reach up to 40° [9]. Therefore, a method was proposed to take into account this rotation for real-life applications. The IMU at C7 was placed on the body in a way that its coordinate system (x_{SCS}, y_{SCS}, and z_{SCS}) best matches the body-fixed coordinate system (right-front-up). At each time step, the local coordinate system of the IMU at C7 was reoriented using the corresponding IMU-measured quaternions in a way that z_{SCS} matches z_{LCS} (and therefore x_{SCS} and y_{SCS} are in the transverse plane). These reoriented axes are denoted as x^*_{SCS}, y^*_{SCS} and z^*_{SCS}. The z^*_{SCS} axis is vertical and is considered to represent z_{BCS}. As trunk rotates around z_{BCS} while walking, the average orientation of the y^*_{SCS} in transverse plane during each gait cycle was assumed to represent the walking direction, and therefore y_{BCS}, for that gait cycle. x_{BCS} is then found perpendicular to these y_{BCS} and z_{BCS}, towards the right of the body to form the right-handed coordinate system.

The acceleration signals measured by each IMU were initially reoriented from SCS to LCS using the orientation (quaternions) measured by the corresponding IMU. At each time-step, the horizontal angle β between y_{LCS} and y_{BCS} at C7 was calculated to represent the 'heading' of the body with respect to LCS while walking. β was then used to reorient (rotate around z_{LCS}) the IMUs accelerations from the LCS to BCS.

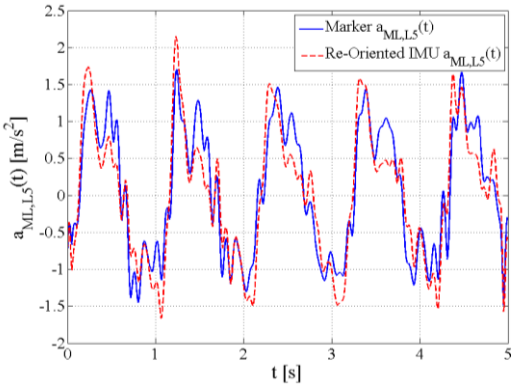

Fig. 2. Comparison of ML IMU accelerations with the corresponding marker data at L5

These accelerations in BCS were used in this study to estimate the ground reaction forces in the vertical (V – along z_{BCS}), anterior-posterior (AP – along y_{BCS}) and medial-lateral (ML – along x_{BCS}) direction. Fig. 2 illustrates a typical example of IMU medial-lateral accelerations reoriented to BCS in comparison with the corresponding accelerations measured by the motion capture system at L5. The accuracy of the IMU orientations were deemed acceptable after comparing the re-oriented IMU accelerations and the motion capture data in BCS (Fig. 2). This is mainly attributed to the successful performance of the internal Kalman filter of the Opal IMUs to reject magnetic disturbances when using magnetic field to calculate IMU orientation.

The human body was represented as an articulated multi-segment 3D system with 13 rigid segments: head, torso, pelvis, upper arms, forearms, thighs, shanks and feet. The anthropometric data for each body segment including anatomical coordinate systems, joint centre definitions, the segmental masses and their CoM location are based on the system suggested by Ren, et al., [10] and Winter [1].

The motion capture system was calibrated to measure motion in BCS and treadmill was aligned with the y_{BCS} axis. All the measured data were re-sampled at 100Hz and synched using MATLAB software [11]. The raw kinematic data (tri-axial displacements) were filtered using a low pass zero lag fourth-order Butterworth digital filter with a cut off frequency of 12Hz to remove high-frequency noise while preserving the frequency contents corresponding to the first four harmonics and sub-harmonics of the walking $GRF(t)$ signals. The displacement signals were then double differentiated to find the corresponding acceleration signals. Before each differentiation, signals were low pass filtered using the mentioned Butterworth filter, to reduce the high frequency noise associated with the differentiation process [12].

These tri-axial acceleration signals, calculated for all CODA markers on the body, were subsequently used to calculate the acceleration $\ddot{x}_{j,i}(t)$ of the CoM of each segment 'i' in direction 'j' based on the CoM locations proposed by Ren, et al., [10] and Winter [1].

III. Relation of Total GRF Signals and Body Kinematics

Based on the second Newton law and assuming that body is comprised of n solid segments, walking $GRF_j(t)$ signals (excluding the static body weight in the vertical direction) in each direction 'j' can be estimated using (2):

$$GRF_j(t) = \sum_{i=1}^{n}(m_i \times \ddot{x}_{j,i}(t)), \qquad j \in [V, AP, ML], \tag{2}$$

where, m_i is the segment 'i' mass. If errors associated with assuming solid body segments, frictionless pin joints, soft tissue artifacts, and anthropometric measurements [1] are assumed negligible, (2) theoretically give an accurate estimation of the total $GRF(t)$ signals in each direction. However, even if this assumption is deemed acceptable, it is impractical to measure acceleration of all body segments on long-term basis and number of sensors has to be minimized.

A. Correlation analysis

To find the optimal locations on the body for IMU sensors, the Pearson linear correlation coefficient r between $\ddot{x}_{j,i}(t)$ and corresponding treadmill-measured total $GRF_j(t)$ signals were calculated for each test and their average values across all 25 tests are compared in Fig. 3. The cross-correlation coefficients in this figure for body segments 'i' and 'p' were calculated using (3) and (4) [13] and [14]:

$$r\left(GRF_j(t), \ddot{x}_{j,i}(t)\right) = \frac{1}{N-1}\sum_{n=1}^{N}\left(\frac{GRF_j(t_n)-\overline{GRF_j}(t)}{\sigma_{GRF_j(t)}}\right)\left(\frac{\ddot{x}_{j,i}(t_n)-\overline{\ddot{x}_{j,i}}(t)}{\sigma_{\ddot{x}_{j,i}(t)}}\right), \tag{3}$$

$$r\left(\ddot{x}_{j,i}(t), \ddot{x}_{j,p}(t)\right) = \frac{1}{N-1}\sum_{n=1}^{N}\left(\frac{\ddot{x}_{j,i}(t_n)-\overline{\ddot{x}_{j,i}}(t)}{\sigma_{\ddot{x}_{j,i}(t)}}\right)\left(\frac{\ddot{x}_{j,p}(t_n)-\overline{\ddot{x}_{j,p}}(t)}{\sigma_{\ddot{x}_{j,p}(t)}}\right). \tag{4}$$

In these equations, $\sigma_{GRF_j(t)}$, $\sigma_{\ddot{x}_{j,p}(t)}$ and $\sigma_{\ddot{x}_{j,i}(t)}$ are the standard deviation of $GRF_j(t)$, $\ddot{x}_{j,p}(t)$ and $\ddot{x}_{j,i}(t)$ signals, respectively, and $\overline{GRF_j}(t)$, $\overline{\ddot{x}_{j,p}}(t)$ and $\overline{\ddot{x}_{j,i}}(t)$ are the mean value of signals over N samples.

As can be seen in Fig. 3, in the vertical direction, the cross-correlation of $GRF_v(t)$ and $\ddot{x}_{v,i}(t)$ signals increases from feet to head. This correlation is highest at the head with the

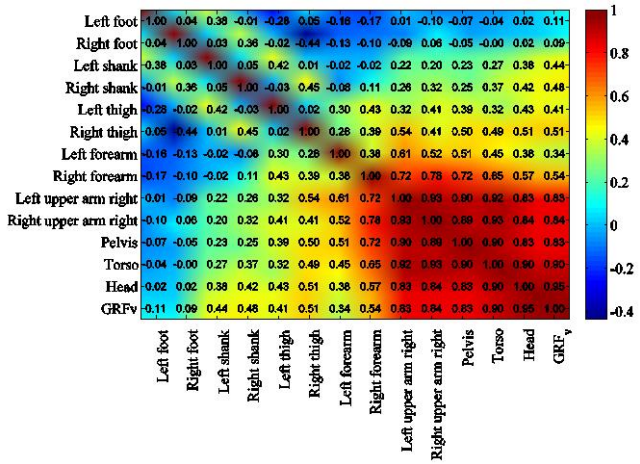

a)

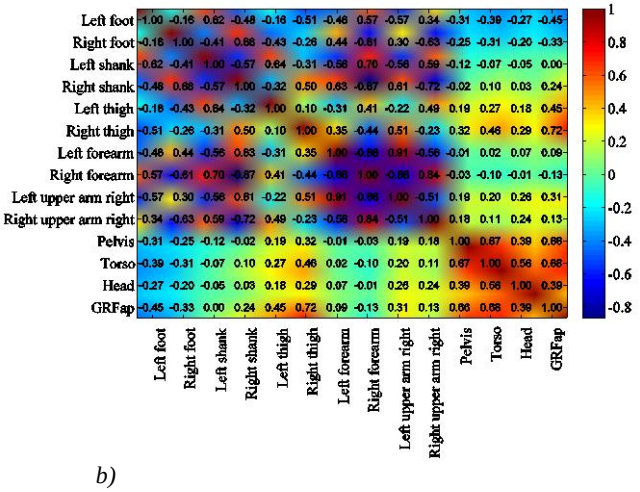

b)

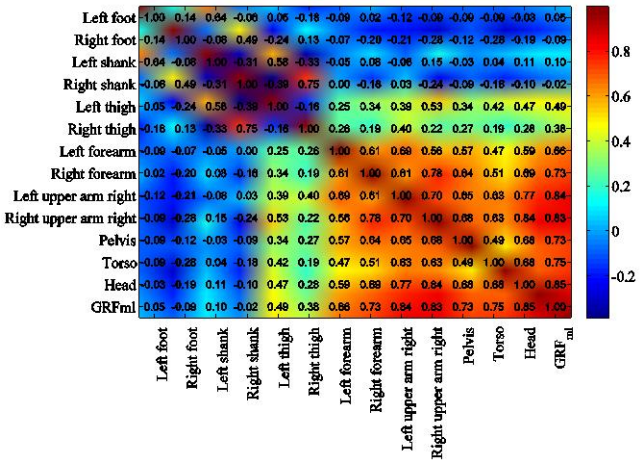

c)

Fig. 3. Pearson coefficients of correlation between the $GRF_j(t)$ and $\ddot{x}_{j,i}(t)$ signals in the (a) vertical, (b) anterior-posterior and (c) medial-lateral directions.

average value of 0.95. However, head and arms were deemed unreliable locations for acceleration measurement as their frequent intentional movements are often uncorrelated with the movement of the body CoM and this create significant errors in estimated walking $GRF(t)$ signals. The second highest correlation with $GRF_v(t)$, but without uncorrelated movement errors, corresponds to the torso CoM. In the AP direction, the $\ddot{x}_{ap,i}(t)$ pertinent to pelvis, torso and thighs showed the highest correlation with $GRF_{ap}(t)$, whereas, the $\ddot{x}_{ml,i}(t)$ of the upper arms and head and then torso and pelvis found to have the highest correlation with $GRF_{ml}(t)$.

B. Contribution analysis

Based on (2), contribution of each segment *'i'* to $GRF_j(t_n)$ in direction *'j'* and at time step t_n is defined as:

$$Con_{j,i}(t_n) = [\frac{m_i \times \ddot{x}_{j,i}(t_n)}{GRF_j(t_n)}] \times 100. \quad (5)$$

Fig. 4 illustrates the $Con_{j,i}(t_n)$ ratios in the V (a), AP (b) and ML (c) directions during a stance phase. The contribution ratios presented in this figure are the average values of all stance cycles extracted from all 25 tests. As it can be seen in this figure, torso and then thighs had the highest contribution to $GRF_v(t)$. Similarly, thighs and torso showed the highest contribution to $GRF_{ap}(t)$ and $GRF_{ml}(t)$, respectively. These

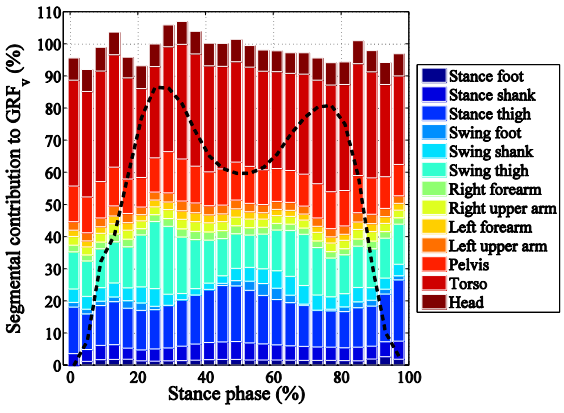

a)

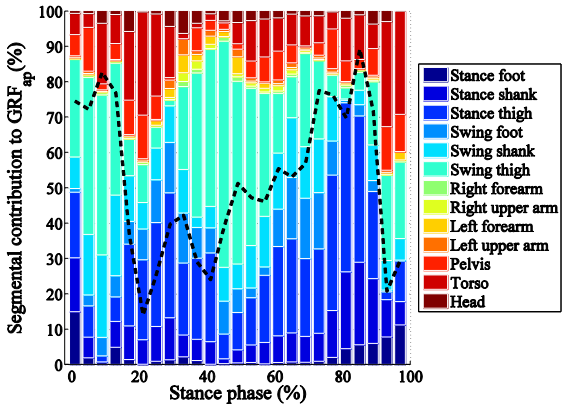

b)

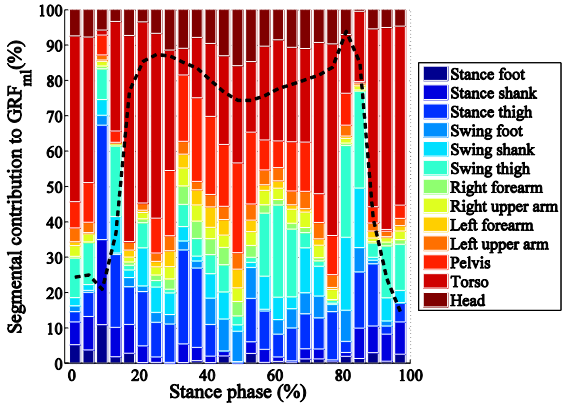

c)

Fig. 4. Segmental contribution to the total $GRF_j(t)$ signals in the (a) vertical, (b) anterior-posterior and (c) medial-lateral directions

segments happen to be the heaviest body segments which indicates the critical effects of their mass in (2) and (5). Another interesting observation from Fig. 4 is that the magnitude of the contribution of segments are much more uniform throughout the stance cycle in the vertical direction compared with the AP and ML directions. In AP direction, the swing thigh dominates the contribution during mid-stance and most of the terminal stance until the stance thigh dominates the contribution during pre-swing.

C. Spectral analysis

The contribution $Con_{j,i}(t_n)$ of each segment to measured $GRF_j(t)$ was also analyzed in the frequency domain. Due to the variation of pacing frequency f_p in each test and its effects on the spectrum of $GRF_j(t)$ signals, it was not possible to average the spectrums pertinent to different tests. Fig. 5a, c and e show the absolute Fourier spectrum (disregarding phase data) of $m_i \times \ddot{x}_{j,i}(t_n)$, and Fig. 5b, d and f show the absolute Fourier spectrum of the corresponding measured $GRF_j(t)$ signals in the V, AP and ML directions, respectively, for S1 test with normal walking speed ($1.25m/s$). As it can be seen in Fig. 5a and b, in the vertical direction, the even walking harmonics (*h=2, 4, 6, 8 & 10*) were dominant in the $GRF_v(t)$ signal and torso was the main contributor to the spectral amplitude at these harmonics. Thighs were found to have the maximum absolute contribution to the $GRF_v(t)$ signal at odd

harmonics (*h=1, 3, 5, 7 & 9*). However, the close to 180 degrees phase difference (antiphase) between the vertical acceleration of right and left thigh at odd harmonics cancelled out each other's contribution and the resultant odd harmonics amplitude of the $GRF_v(t)$ signal (Fig. 5b) were close to zero.

In the AP direction, as is shown in Fig. 5c and d, the even harmonics were again dominant in the $GRF_{ap}(t)$ signal, but thighs had the maximum absolute contribution in all harmonics. However, similar to the vertical direction, the antiphase acceleration of the right and left thighs in the AP direction cancelled out each other's force to high extent and the resultant spectral amplitude of the $GRF_{ap}(t)$ signal at all harmonics (Fig. 5d) were dominated by torso, pelvis and head.

In the ML direction (Fig. 5e and f), contrary to the vertical and AP directions, the odd harmonics were dominant and torso was the main contributor. The anti-phase movements of thighs in the ML direction was responsible for the near zero spectrum of the $GRF_{ml}(t)$ signal at even harmonics (Fig. 5f).

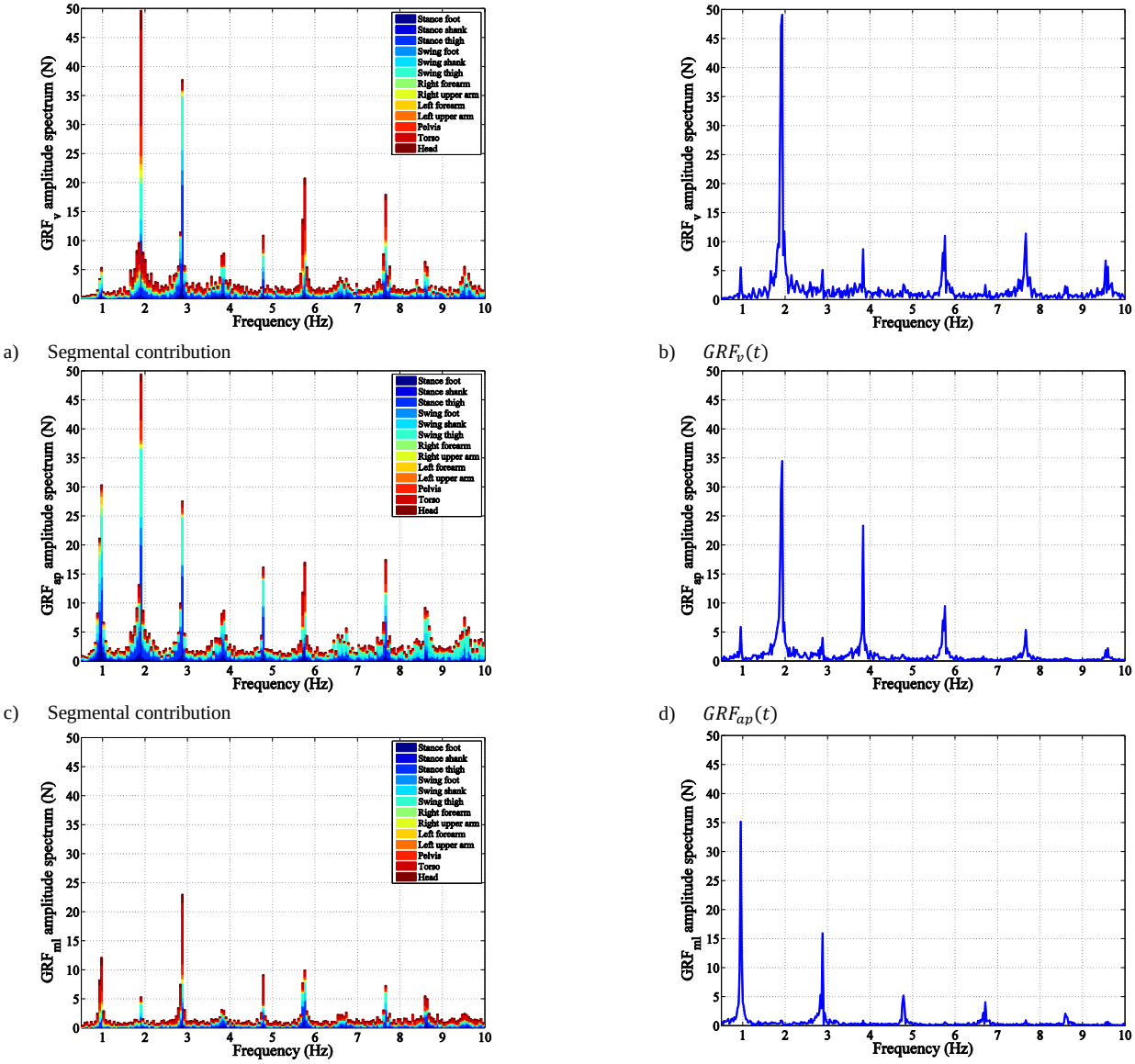

a) Segmental contribution

b) $GRF_v(t)$

c) Segmental contribution

d) $GRF_{ap}(t)$

e) Segmental contribution

f) $GRF_{ml}(t)$

Fig. 5. Spectrum of the segmental contribution to the total $GRF_j(t)$ signals in the (a and b) vertical, (c and d) anterior-posterior and (e and f) medial-lateral directions

D. Discussion

Based on the results of the correlation and contribution analysis, torso, pelvis and thighs are the key body segments for estimating $GRF_j(t)$ signals using models based on (2). In theory, measuring directly the $\ddot{x}_{j,i}(t)$ signals on these segments, rather than estimating them, can potentially minimize the total error in the estimated $GRF_j(t)$ signals.

IV. SENSORY SYSTEM DESIGN

To ensure the *practicality* of the sensory system for continuous real-life measurement, only the systems with maximum three IMUs were considered in this study. Taking into account the insights from Section III, the nonlinear autoregressive moving average model with exogenous inputs (NARMAX) method was used for optimizing the sensors

location and for identification of benchmark mathematical models to estimate $GRF_j(t)$ signals from IMU measurements. The NARMAX model identifies the structure of the model in mathematical form by finding the most important mathematical terms (i.e. inputs) of the model in descending order of contribution until a desired accuracy is achieved [15]. This makes it possible to rank the measurement locations on the body based on their significance for estimating $GRF_j(t)$ signals. A typical NARMAX model is defined in the form of:

$$y(k) = F\big[y(k-1), y(k-2), \dots, y\big(k-n_y\big), u(k-d), u(k-d-1), \dots, u(k-d-n_u), e(k-1), e(k-2), \dots, e(k-n_e)\big] + e(k), \quad (6)$$

where, $y(\cdot)$, $u(\cdot)$ and $e(\cdot)$ are the system's output, input and noise sequences, respectively, and n_y, n_u and n_e are their corresponding maximum lags. The noise terms are included to accommodate the effects of measurement and modelling errors, and unmeasured disturbances. $F[\cdot]$ is some non-linear function and d is a time delay that typically is set to $d = 1$.

To identify the most important sensor locations to estimate each $GRF_j(t)$ signal, for each test, the directly measured acceleration signals from all CODA markers and IMU sensors in direction *'j'* (Fig. 1) were defined as potential input signals $u_1(k) \dots u_m(k)$ and the corresponding treadmill-measured $GRF_j(t)$ signal was defined as the output $y(k)$. Then the inputs with the highest contribution for estimation of $GRF_j(t)$ signal were identified. Fig. 6 illustrates the location of the most important sensors, identified by the NARMAX method, for one, two and three sensors systems in the vertical (Fig. 6a), anterior-posterior (Fig. 6b) and medial-lateral (Fig. 6c) directions for all 25 tests. The color map in Fig. 6 represents the peak-to-peak normalized root mean square error (NRMSE) corresponding to each model and test, calculated as:

$$NRMSE\ (\%) = \frac{\sqrt{\left(\sum_{t=0}^{t_{end}}\left[\left(GRF_{j,measured}(t) - GRF_{j,estimated}(t)\right)^2\right]\right)/N}}{\max\left(GRF_{j,measured}(t)\right) - \min\left(GRF_{j,measured}(t)\right)} \times 100, \quad (7)$$

where, t is the time vector with N samples, starting at zero and ending at t_{end}.

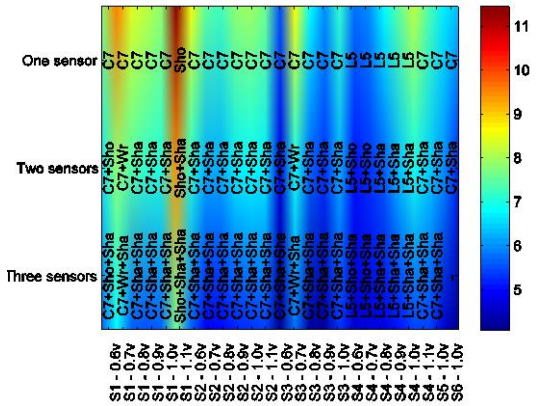

a)

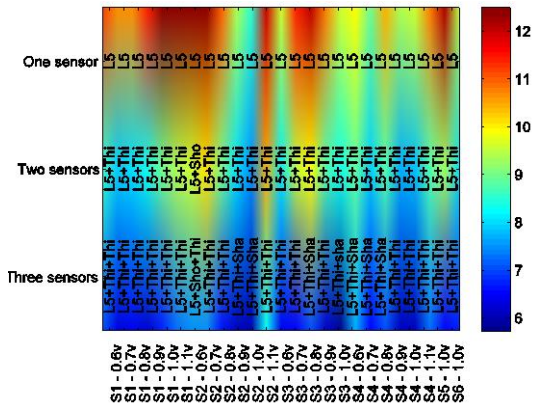

b)

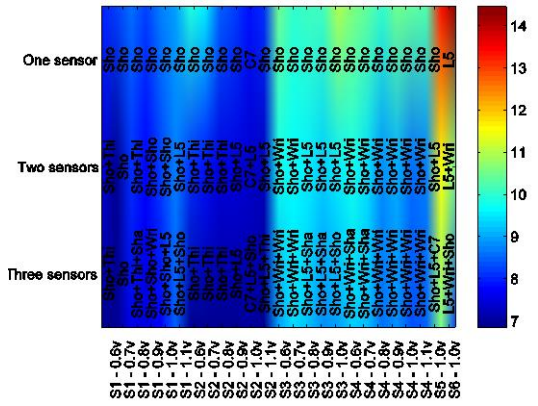

c)

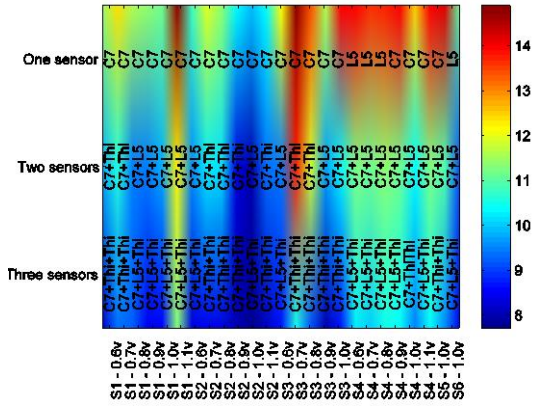

d)

Fig. 6. Optimal location of IMUs to estimate $GRF_j(t)$ in the V(a), AP(b), and ML(c) directions and to estimate (d) tri-axial $GRF_j(t)$ signals.

As it can be seen in Fig. 6a, in the vertical direction, C7 for the single sensor system, C7 and one of the shanks for the two sensors system and C7 and both shanks for the three sensors system appear more frequently than other combinations and, therefore, are identified as the best locations for IMUs to measure $\ddot{x}_{v,i}(t)$ for estimation of $GRF_v(t)$. Similarly, to estimate $GRF_{ap}(t)$ (Fig. 6b), L5 for the single sensor system, L5 and one of the thighs for the two sensors system and, L5 and both thighs for the three sensors system are the optimal IMU locations. The IMU locations identified in ML direction (Fig. 6c) were not as coherent across all 25 tests as were in the V and AP directions. Overall, $\ddot{x}_{ml,i}(t)$ measured at one of the shoulders seems the best candidate to estimate $GRF_{ml}(t)$.

In the next step, the optimal location for IMUs to estimate all three components of the $GRF_j(t)$ signals were identified and are shown for all 25 tests in Fig. 6d. As it can be seen in this figure, C7 for the single sensor system, C7 and L5 for the two sensors system and C7, L5 and one of the thighs for the three sensors system were identified as the best locations for IMUs.
In all four cases, the higher the number of sensors was, the lower was the NRMSE of the estimated $GRF_j(t)$ signals. The average decrease in these NRMSEs, by increasing the number of sensors from one to three, were 2%, 3%, 3% and 4% for V, AP, ML and tri-axial directions, respectively.

V. Linear models to estimate total GRFs

This study only focuses on developing models for the three sensors system with IMUs at C7, L5 and one of the thighs. This is because while being practical, such system provides the highest accuracy in results compared with the one and two sensor(s) systems. Twenty randomly selected tests from S1-S4 were used for model development. The remaining three tests from S1-S4 were used for intra-subject validation and the two tests pertinent to S5 and S6 were used for inter-subject validation. Motion capture data were used for developing the models presented in Sections V.A, V.B, V.C, and VI, while IMU measurements were used in Sections V.D and VII.
The system identification procedure was started with a simple linear model with the structure based on (2). The general form of the linear model was taken as:

$$GRF_j(t) = \left(\alpha_{j,c7} \times \ddot{x}_{j,C7}(t)\right) + \left(\alpha_{j,L5} \times \ddot{x}_{j,L5}(t)\right) + \left(\alpha_{j,Thi} \times \ddot{x}_{j,Thi}(t)\right), \quad (8)$$

where, $j \in \{V, AP, ML\}$ and α represents part of the total body mass represented by each IMU and calculated as discussed in the next Sections:

$$m_{total} = \alpha_{j,c7} + \alpha_{j,L5} + \alpha_{j,Thi} \quad (9)$$

Two linear models are proposed in this section to estimate α, based on (8). The accuracy of the tri-axial $GRF_j(t)$ signals estimated using these two models are later compared with those of the NARMAX model of the same structure.

A. Model 1

For each direction *'j'*, the Pearson cross-correlation coefficients $r_{j,i,p}$ between acceleration signal $\ddot{x}_{j,i}(t)$ of CoM of each segment '*i*' and the corresponding IMU signals $\ddot{x}_{j,p}(t)$ measured at C7, L5 and one of the thighs (denoted as p) were calculated using (4). Model 1 proposes to use (10)-(12), in each direction 'j', to calculate the α coefficients in (8):

$$\alpha_{j,C7} = \sum_{i=1}^{13}\left(\frac{r_{j,i,C7}}{r_{j,i,C7}+r_{j,i,L5}+r_{j,i,Thi}} \times m_i\right) \quad (10)$$

$$\alpha_{j,L5} = \sum_{i=1}^{13}\left(\frac{r_{j,i,L5}}{r_{j,i,C7}+r_{j,i,L5}+r_{j,i,Thi}} \times m_i\right) \quad (11)$$

$$\alpha_{j,Thi} = \sum_{i=1}^{13}\left(\frac{r_{j,i,Thi}}{r_{j,i,C7}+r_{j,i,L5}+r_{j,i,Thi}} \times m_i\right) \quad (12)$$

B. Model 2

Model 2 utilizes the same $r_{j,i,p}$ correlation coefficients, and proposes (13) - (15) to calculate the α coefficients in (8) for each direction *'j':*

$$\alpha_{j,C7} = \sum_{i=1}^{13}\begin{cases} m_i & if\ r_{j,i,C7}\ is \max(r_{j,i,C7}, r_{j,i,L5}, r_{j,i,Thi}) \\ 0 & Otherwise \end{cases} \quad (13)$$

$$\alpha_{j,L5} = \sum_{i=1}^{13}\begin{cases} m_i & if\ r_{j,i,L5}\ is \max(r_{j,i,C7}, r_{j,i,L5}, r_{j,i,Thi}) \\ 0 & Otherwise \end{cases} \quad (14)$$

$$\alpha_{j,Thi} = \sum_{i=1}^{13}\begin{cases} m_i & if\ r_{j,i,Thi}\ is \max(r_{j,i,C7}, r_{j,i,L5}, r_{j,i,Thi}) \\ 0 & Otherwise \end{cases} \quad (15)$$

Model 2 maintains that the acceleration signal of the IMU with the highest correlation coefficient $r_{j,i,p}$ represents the acceleration of the body segment *'i'* in the direction *'j'*.

C. NARMAX model

To put the accuracy of the results of the Models 1 and 2 in context, a NARMAX model with the same structure with (8) was identified:

$$y_j(k) = \left(\alpha_{j,c7} \times u_{j,C7}(k)\right) + \left(\alpha_{j,L5} \times u_{j,L5}(k)\right) + \left(\alpha_{j,Thi} \times u_{j,Thi}(k)\right), \quad (16)$$

where, $u_{j,p}(k)$ is the IMU *'p'* acceleration signal in the direction *'j'* and $y_j(k)$ is the corresponding measured $GRF_j(k)$. Results of the NARMAX model were assumed to serve as benchmark values, representing the highest accuracy achievable for the model with the (8) structure.
Equations (10) - (12) for Model 1, (13) - (15) for Model 2 and NARMAX algorithm for the NAMRAX model were first used to calculate the α coefficients for each of 20 tests in three directions. Then the average values of the α coefficients across all 20 tests were used in (8) to estimate the $GRF_j(t)$ signals. The same average α coefficients were also used in (8) to estimate the $GRF_j(t)$ signals for the five control tests. Fig. 7 shows the NRMSE values corresponding to all the 25 tests. The average (standard deviation) of the NRMSE values for training and validation datasets are presented in TABLE I for each model. As it can be seen in TABLE I, the Model 1 NRMSEs pertinent to the AP and ML direction were particularly high. Compared with Model 1, Model 2 estimated the $GRF_j(t)$ signals with 2% and 4% lower NRMSE in the V and AP directions, respectively, and with 11% higher error in the ML direction (inter-subject validation results). Comparing these NRMSE values with those of the NARMAX model, it can be seen that, overall, Model 2 yields closer results to NARMAX results in estimation of $GRF_j(t)$ with (8) structure.

TABLE I: COMPARISON OF MODELS NRMSE(SD)

	V (%)	AP (%)	ML (%)
Model 1 (all trials)	8(1.7)	21(2.2)	16(3.2)
validation intra-subject	9(1.5)	19(2.5)	14(4.5)
validation inter-subject	9(0.7)	20(1.4)	21(2.1)
Model 2 (all trials)	7(1.7)	16(2.0)	18(6.7)
validation intra-subject	7(1.5)	15(1.2)	14(4.4)
validation inter-subject	7(0.0)	16(0.7)	32(2.8)
NARMAX (all trials)	7(1.2)	12(1.5)	14(4.8)
validation intra-subject	7(1.2)	11(0.6)	11(3.6)
validation inter-subject	6(0.0)	12(0.7)	23(0.7)
Model 2 with training	7(1.3)	13(2.0)	13(2.8)
NARMAX with training	7(1.2)	9(0.8)	12(3.2)
NL order 1 - 1 lag	5(1.1)	7(0.8)	9(2.3)
NL order 2 - 1 lag	5(1.0)	7(0.8)	9(2.2)

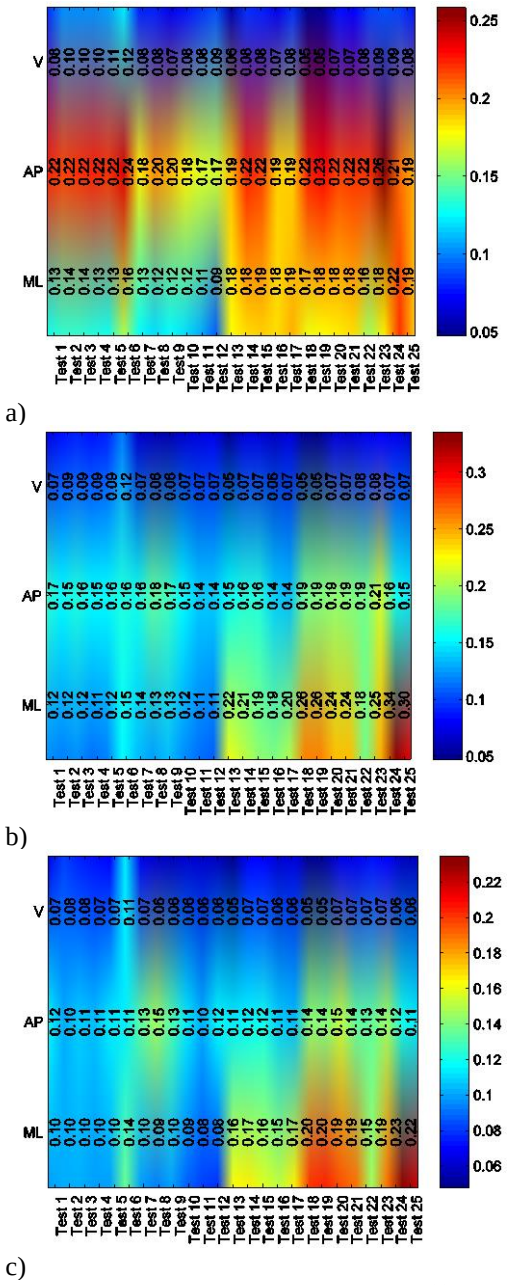

Fig. 7. NRMSE corresponding to the estimated $GRF_j(t)$ signals for (a) Model 1, (c) Model 2 and (d) NARMAX model

D. *Subject-specific training*

A very useful feature of Model 2 is that its α coefficients can be determined only using the acceleration of different body segments (13) - (15). Therefore, it is possible to train the model for each particular subject, walking regime or gait pattern only using IMUs, assuming that for each body segment, a location for IMU can be found to measure the acceleration of CoM of that segment, with reasonable accuracy. Such subject/gait-specific training can significantly enhance the accuracy of the estimated $GRF_j(t)$ signals while maintaining its practicality.

To analyze the effects of the subject/gait-specific training on the performance of the model, IMU measurements were used to calculate the α coefficients of Model 2 for each of the 25 tests in three directions using (13) - (15). The IMU measurements at pelvis, upper arms, forearms, thighs, shanks and feet were used to represent the acceleration of these segment and the acceleration of head and torso were assumed to be represented by C7. The α coefficients pertinent to each test were then used to estimate the $GRF_j(t)$ signals of that particular test and the corresponding NRMSE values were calculated. Fig. 8 compares typical measured and estimated $GRF_j(t)$ signals for Subject 1 walking with comfortable speed (Test 5). As it can be seen in this figure, the model estimated $GRF_j(t)$ reasonably well. The noticeable error in every other local minima of the estimated $GRF_{ap}(t)$ (Fig. 8b) is mainly due to the fact that $GRF_{ap}(t)$ relies on the measured acceleration of both thighs as mentioned in Sections III and IV. However, in the 3-IMU system used in this section, only the acceleration measured from one of the thighs is available to the model. If an IMU is added to the other thigh as well, the NRMSE error would decrease from 13% (TABLE I) to 10% for the estimated $GRF_{ap}(t)$.

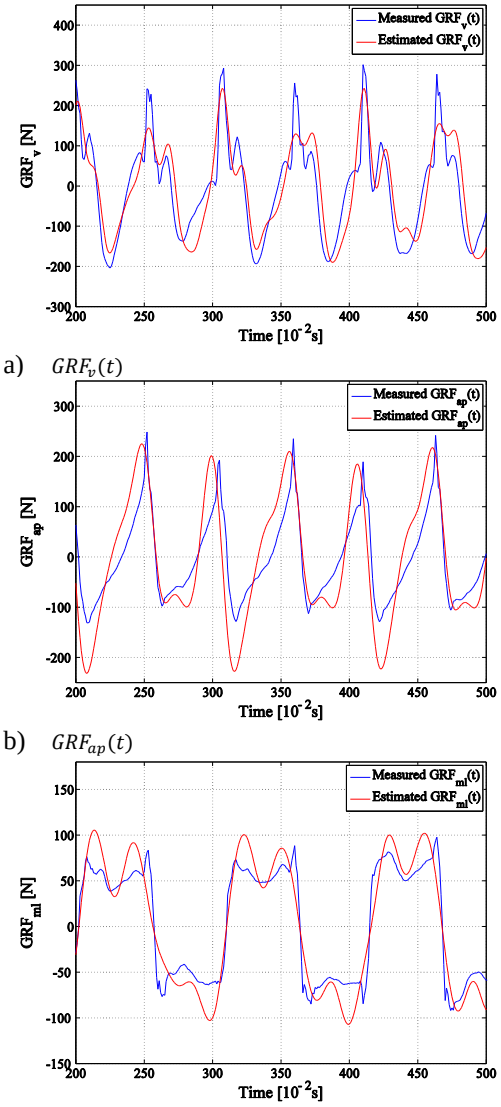

Fig. 8. A typical comparison of measured and estimated $GRF_j(t)$ in the V (a), AP (b) and ML (c) directions for Subject 1 walking with comfortable speed (Test 5)

The NRMSE value corresponding to each test are compared in Fig. 9a. Compared with the Model 2 results without test-specific training (Section B), these NRMSE values represent significant reduction of 3% and 5% (all trials) in AP and ML directions, respectively. These NRMSE values further compare favorably with the NRMSE values for the NARMAX model with test-specific training (Fig. 9 - TABLE I).

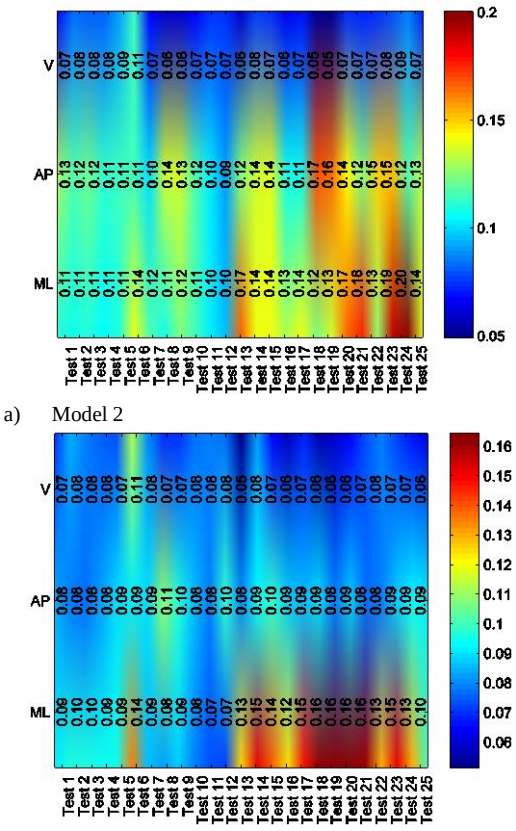

a) Model 2

b) NARMAX

Fig. 9. (a) Model 2 and (b) NARMAX NRMSE with test-specific training

VI. Non-linear models

The possibility of improving the accuracy of the estimated $GRF_j(t)$ signals are explored in this section using NARMAX by introducing two forms of mathematical non-linearity in the model by allowing the polynomial NARMAX model: (1) to assume second order, and (2) to use the lagged terms of the input signals up to five lags i.e. $u(k-1), \dots, u(k-5)$. The linear models discussed in Section V with (8) structure are a sub-class of this general non-linear structure where the polynomial order is one and no lag is permitted. For each of the 25 tests in each direction *'j'*, the IMU measurements $\ddot{x}_{j,C7}(t)$, $\ddot{x}_{j,L5}(t)$ and $\ddot{x}_{j,Thi}(t)$ were used as input to NARMAX and a non-linear model was identified to estimate the corresponding $GRF_j(t)$ signal. The NRMSE pertinent to each test in each direction *'j'* was calculated and their average value across all 25 tests are shown in Fig. 10. This procedure was repeated for the polynomials of first and second order and for the maximum allowable lagged term of 1-5.

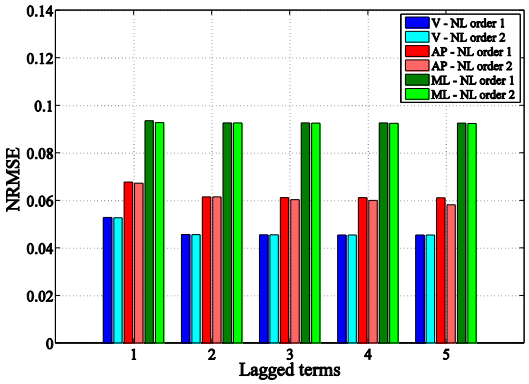

Fig. 10. Comparison of the accuracy of the linear and non-linear models

As it can be seen in Fig. 10 and TABLE I, NARMAX models with one lagged term estimated the $GRF_j(t)$ signals with 2%, 2% and 3% less NRMSE in the vertical, AP and ML directions, respectively, compared with the corresponding linear NARMAX model with test-specific training. The accuracy of the estimated $GRF_j(t)$ signals for both first and second order models, however, found to be very similar. This can be interpreted as the relationships between $\ddot{x}_{j,p}(t)$ and corresponding $GRF_j(t)$ signals are to high extent linear. On the other hand, increasing the number of allowed lagged terms in the model beyond one, increased the accuracy of the estimated $GRF_j(t)$ signals by maximum 1% NRMSE. However, involving lagged terms complicates the structure of the model and the model structure will no longer be physically interpretable based on (2).

VII. Real-life validation

Walking gait in real-life environment is characterized with high variability in magnitude and timing compared with the treadmill-measured $GRF_j(t)$ signals. To analyze the performance of the Model 2 in real-life environment, a set of tests was carried out where 10 subjects walked around the University of Sheffield campus buildings (in paved urban environment), while wearing a pair of Tekscan F-Scan in-shoe pressure insoles [16]. The walking pathway was characterized with flat parts as well as uphills and downhills. Subjects were asked to walk normally, and no further instructions were given to keep the experiments as realistic as possible.

Body acceleration was measured using three IMUs at C7, L5 and one of the thighs. The normal plantar pressures measured under both feet were used to calculate the left foot, right foot and the total $GRF_v(t)$, signals. Before and after each trial, subjects walked with their normal speed on the instrumented treadmill while wearing pressure insoles and the $GRF_v(t)$ signals measured by the treadmill were used to calibrate the pressure insole measurements for each outdoor walking test.

Model 2 with subject-specific training was used to estimate the total $GRF_v(t)$ signals for each subject. Before each outdoor test, a set of 13 walking measurements, each with 30s duration, were carried out to determine subject-specific α coefficients for each test subject. In these measurements, three IMUs were placed at C7, L5 and the right thigh, while in each test the fourth IMU was placed closest to the approximate location of the CoM of one of the body segments '*j*' and the

corresponding $\alpha_{j,C7}$, $\alpha_{j,C7}$, and $\alpha_{j,C7}$ coefficients were calculated using Equations (13) - (15).

A set of 115 data segments of 5s duration were randomly extracted from the measured outdoor data for analysis. Both Model 2 and the Equation 1 were used to estimate the total $GRF_v(t)$ signal for each of 5s time histories and the corresponding NRMSE values were calculated. Fig. 11a compares the distribution of the NRMSE values for Model 2 and Equation 1. Model 2 shows mean NRMSE of 8.7% compared with 10.3% for Equation 1 results, and compares favorably with the treadmill tests results (mean 7% NRMSE). Fig. 11b and c show the measured $GRF_v(t)$ time histories with the worse and best $GRF_v(t)$ estimates, respectively. As it can be seen in Fig. 11b, the high frequency peaks of $GRF_v(t)$ are not estimated accurately by Model 2 in the worst estimate.

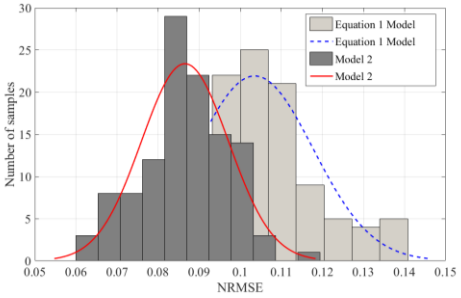

a) NRMSE distribution

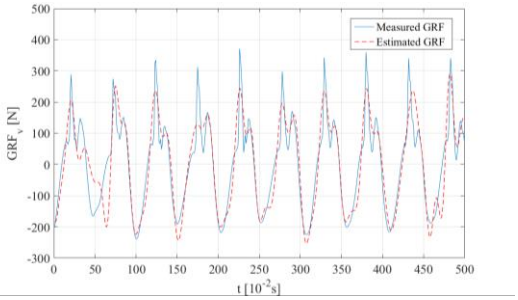

b) Worse estimate NRMSE: 0.119

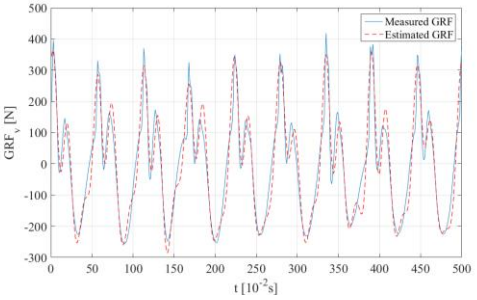

c) Best estimate NRMSE: 0.062

Fig. 11. Performance of the Model 2 in outdoor environment

VIII. CONCLUSIONS

The present paper studied in detail the correlation between the acceleration of the body segments and the $GRF_j(t)$ signals in three directions using a set of 25 walking gait measurements on six subjects. Using the NARMAX system identification model, it was found that for estimation of the tri-axial $GRF_j(t)$ signals, C7 for the single IMU system, C7 and L5 for the two IMUs system and C7, L5 and one of the thighs for the three IMUs system are the optimal locations on the body to measure tri-axial acceleration.

A linear model based on the correlation of the segmental accelerations and the IMU measurements was proposed that can be trained easily for each subject and gait pattern using only IMUs. This model estimated $GRF_j(t)$ with average 7%, 13% and 13% NRMSE in the vertical, AP and ML directions, respectively. It was further shown that for the dataset used in this study, the first-order non-linear model with one lagged term showed 2-3% reduction in NRMSE compared with the corresponding linear model.

The main limitations of this study are: (1) models were developed and validated only for healthy subjects and pathological gaits were not considered, and (2) the validation dataset was small. A larger dataset, statistically representative of a wide spectrum of gait patterns, subject parameters (age, height, weight, etc.) and gait conditions is needed to validate, personalize and enhance the proposed models.

REFERENCES

[1] D. A. Winter, "The biomechanics and motor control of human gait: normal, elderly and pathological," University of Waterloo press, Ontario, 1991.

[2] M. G. McDonald, and S. Zivanovic, "Measuring Dynamic Force of a Jumping Person by Monitoring Their Body Kinematics," In proceeding of 11th International Conference on Recent Advances in Structural Dynamics (RASD), Italy, 2013.

[3] M. Bocian, J. M. W. Brownjohn, V. Racic, D. Hester, A. Quattrone, and R. Monnickendam, "A framework for experimental determination of localized vertical pedestrian forces on full-scale structures using wireless attitude and heading reference systems," Journal of Sound and Vibration. vol. 376, pp. 217–243, 2016. http://dx.doi.org/10.1016/j.jsv.2016.05.010

[4] R. D. Gurchiek, R. S. McGinnis, A. R. Needle, J. M. McBride, and H. Werkhoven, "The use of a single inertial sensor to estimate 3-dimensional ground reaction force during accelerative running tasks," Journal of Biomechanics. Vol. 61, pp. 263-268, 2017.

[5] Charnwood Dynamics Limited, "Coda motion user's manual," Coda motion website: http://www.codamotion.com/index.php/applications/hardware/item/127-cx1-3d-scanners, 2016.

[6] Vicon Motion Systems, "Bonita motion capture system data sheet," Accessed online at 28/10/2016 at: https://www.vicon.com/file/vicon/bonita-brochure.pdf.

[7] APDM, "Mobility lab white paper," Accessed online at 28/10/2016 at APDM website: http://www.apdm.com/wp-content/uploads/2015/10/Whitepaper1.pdf.

[8] C. Y. Chung, M. S. Park, S. H. Lee, S. J. Kong, and K. M. Lee, "Kinematic aspects of trunk motion and gender effect in normal adults" Journal of NeuroEngineering and Rehabilitation, Vol. 7, 9, 2010.

[9] J. Pavčič, Z. Matjačić, and A. Olenšek, "Kinematics of turning during walking over ground and on a rotating treadmill" Journal of NeuroEngineering and Rehabilitation, Vol. 11, 127, 2014.

[10] L. Ren, R. K. Jones, and D. Howard, "Whole body inverse dynamics over a complete gait cycle based only on measured kinematics," Journal of Biomechanics, vol. 41, 2008.

[11] MathWorks, "MATLAB and Statistics Toolbox Release 2016," The MathWorks, Inc., Natick, Massachusetts, United States, 2016.

[12] W. Zijlstra, "Assessment of spatio-temporal parameters during unconstrained walking," European Journal of Applied Physiology, vol. 92, pp .39–44, 2004. doi: 10.1007/s00421-004-1041-5.

[13] R. A. Fisher, "Statistical Methods for Research Workers," 13th edition, Hafner, 1958.

[14] M. G. Kendall, "The Advanced Theory of Statistics," 4th Ed., Macmillan, 1979.

[15] Billings, S. A, Nonlinear system identification: NARMAX methods in the time, frequency, and spatio-temporal domains, John Wiley & Sons Ltd, 2013, ISBN: 978-1-119-94359-4

[16] Tekscan. F-Scan® In-Shoe Analysis System data sheet.